

ARTICLE OPEN

Oxidized-monolayer tunneling barrier for strong Fermi-level depinning in layered InSe transistors

Yi-Hsun Chen¹, Chih-Yi Cheng¹, Shao-Yu Chen^{1,2}, Jan Sebastian Dominic Rodriguez³, Han-Ting Liao⁴, Kenji Watanabe¹, Takashi Taniguchi⁵, Chun-Wei Chen⁴, Raman Sankar^{6,7}, Fang-Cheng Chou⁶, Hsiang-Chih Chiu³ and Wei-Hua Wang^{1*}

In two-dimensional (2D)-semiconductor-based field-effect transistors and optoelectronic devices, metal–semiconductor junctions are one of the crucial factors determining device performance. The Fermi-level (FL) pinning effect, which commonly caused by interfacial gap states, severely limits the tunability of junction characteristics, including barrier height and contact resistance. A tunneling contact scheme has been suggested to address the FL pinning issue in metal–2D-semiconductor junctions, whereas the experimental realization is still elusive. Here, we show that an oxidized-monolayer-enabled tunneling barrier can realize a pronounced FL depinning in indium selenide (InSe) transistors, exhibiting a large pinning factor of 0.5 and a highly modulated Schottky barrier height. The FL depinning can be attributed to the suppression of metal- and disorder-induced gap states as a result of the high-quality tunneling contacts. Structural characterizations indicate uniform and atomically thin-surface oxidation layer inherent from nature of van der Waals materials and atomically sharp oxide–2D-semiconductor interfaces. Moreover, by effectively lowering the Schottky barrier height, we achieve an electron mobility of $2160 \text{ cm}^2/\text{Vs}$ and a contact barrier of 65 meV in two-terminal InSe transistors. The realization of strong FL depinning in high-mobility InSe transistors with the oxidized-monolayer presents a viable strategy to exploit layered semiconductors in contact engineering for advanced electronics and optoelectronics.

npj 2D Materials and Applications (2019)3:49; <https://doi.org/10.1038/s41699-019-0133-3>

INTRODUCTION

Two-dimensional (2D) semiconductors present great potential for electronics and optoelectronics applications due to several unique characteristics, including efficient electrostatics, a lack of short-channel effects, and the absence of dangling bonds.^{1–6} Recent studies revealed that one of the challenges of fabricating 2D-semiconductor-based transistors is to achieve an Ohmic contact at the interface of the electrodes and the 2D semiconductors.^{7–11} In conventional bulk semiconducting devices, the Ohmic contact can be realized by matching the work function of the metals to the bands of the semiconductors.^{12–14} However, Kim et al.¹⁵ have shown a strong Fermi-level (FL) pinning in 2D-semiconductor transistors; i.e., the Schottky barrier height (SBH), Φ_{SB} , is virtually independent of the work function of contact metals, resulting in a lack of tunability of contact resistance as well as the low-field-effect mobility and output current.⁶ Moreover, the polarity of carrier transport cannot be manipulated by varying contact metals,⁶ critically limiting the controllability of carrier extraction in 2D-semiconductor transistors. Mitigating the FL pinning effect is thus an urgent need to manifest the intrinsic nature of 2D semiconductors, to modulate the carrier transport properties, and to improve transistor performance.

A tunneling contact has been suggested to address the FL pinning effect in 2D-semiconductor devices by reducing: (i) disorder-induced gap states (DIGS),^{6,16} (ii) metal-induced gap states (MIGS),^{17–19} and (iii) interface dipoles.²⁰ By inserting an insulating layer between the metal and the semiconductor, the MIGS and interface dipoles can be effectively reduced by blocking the metallic wave function^{17–19} and by neutralizing interface dipoles,²⁰ respectively. In the process of the device fabrication, the

insulating layer can protect the underlying 2D semiconductors from direct bombardment and metal diffusion during the metal deposition, decreasing the DIGS in the metal–2D-semiconductor interface.^{6,16} Previous studies have used metal/insulator/semiconductor (MIS) structure to tune the Φ_{SB} in 2D-semiconductor devices.^{20,21} However, these studies presented limited FL depinning, suggesting the difficulties to achieve a high-quality tunneling layer at the metal–semiconductor junctions. We overcome these issues by utilizing a surface oxidation layer (OL) in 2D semiconductors as an effective tunneling barrier. In the in-plane direction, a natively grown OL can yield a high compatibility between the oxide and layered semiconductor,^{22,23} enabling a large-scale and atomically smooth oxide functioned as a tunneling contact in 2D-semiconductor devices. In the out-of-plane direction, because of the nature of van der Waals crystals, the thickness of the oxide layer can be precisely controlled down to atomic-scale resolution, facilitating a high tunability of tunneling efficiency.

In this work, we address the FL pinning effect in 2D-semiconductor-based transistors by demonstrating high-performance indium selenide (InSe) field-effect transistors with an atomically thin, precisely controlled tunneling barrier made by a surface OL. InSe is an emerging 2D semiconducting material with potential applications because of its extraordinary intrinsic characteristics, including a small effective mass in the conduction band, small optical bandgap (1.25 eV), high Hall mobility,^{24,25} and weak electron–phonon scattering.²⁶ Hence, one envisions in InSe a channel material with high electronic performance that validates the demonstration of FL depinning. Here, we fabricate the atomically thin OL by a UV-ozone process that is highly scalable

¹Institute of Atomic and Molecular Sciences, Academia Sinica, Taipei 106, Taiwan. ²School of Physics and Astronomy, Monash University, Clayton, VIC 3800, Australia. ³Department of Physics, National Taiwan Normal University, Taipei 106, Taiwan. ⁴Department of Materials Science and Engineering, National Taiwan University, Taipei 106, Taiwan. ⁵Advanced Materials Laboratory, National Institute for Materials Science, Tsukuba 305-0044, Japan. ⁶Center of Condensed Matter Sciences, National Taiwan University, Taipei 106, Taiwan. ⁷Institute of Physics, Academia Sinica, Taipei 115, Taiwan. *email: wwang@sinica.edu.tw

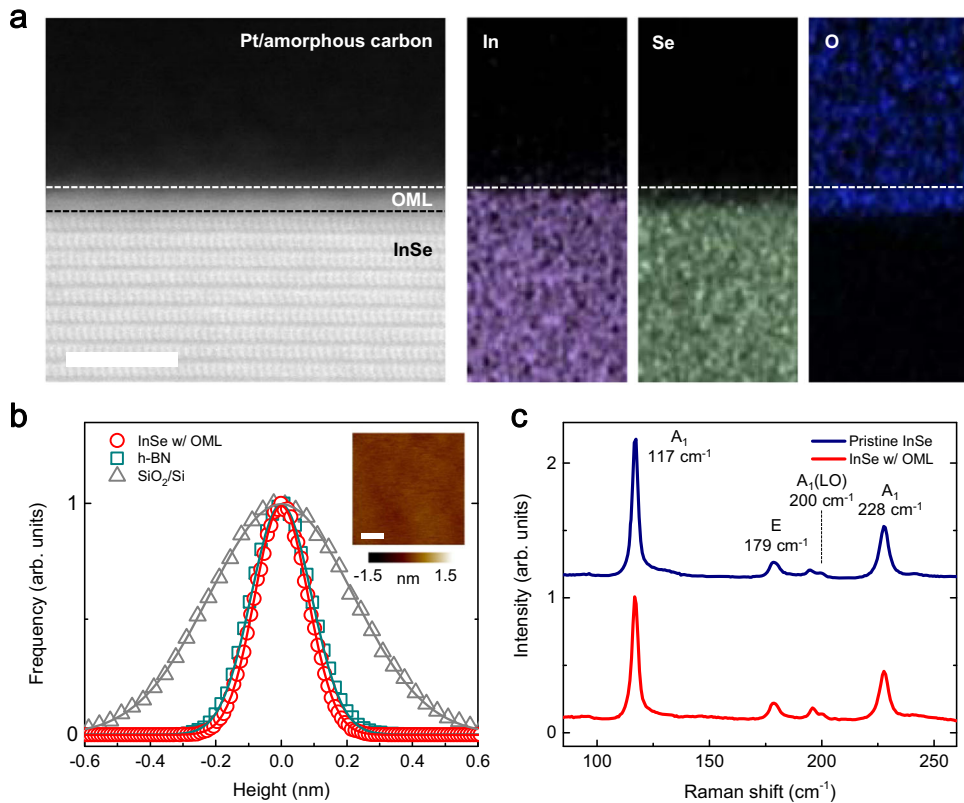


Fig. 1 Material characterizations of the ultra-uniform oxidized-monolayer of InSe. a Cross-sectional transmission electron microscopy and energy-dispersive X-ray spectroscopy mapping images of an InSe sample processed by UV-ozone, showing an atomically sharp, clean interface, and high-crystalline-quality InSe layers underneath the surface OML. The scale bar is 5 nm. **b** A histogram of the height distributions for the surface OML of an InSe sample (red), an h-BN bulk sample (blue), and the SiO_2/Si substrate (green). The solid lines are curves fitted by a Gaussian distribution. The surface roughness values of the InSe surface OML, h-BN bulk, and SiO_2/Si substrate are 81, 91, and 219 pm, respectively. Inset: an AFM image of the surface OML of an InSe sample, showing an ultrasmooth surface morphology. The scale bar is 100 nm. **c** A comparison of the Raman spectra of pristine InSe (blue curve) and the InSe sample with the OML (red curve).

and more compatible with semiconductor manufacturing processes. By employing the surface OL as part of the tunneling contact, we successfully achieve a strong FL depinning in InSe transistors and realize a high-pinning factor of 0.5. Moreover, the barrier height and the threshold voltage can be effectively modulated by varying the work function (WF) of the contact metal because of the pronounced FL depinning. Accordingly, with the selected WF of the contact metal, we achieve a low-contact barrier of 65 meV in the InSe devices, enabling a high two-terminal electron mobility of $2160 \text{ cm}^2/\text{Vs}$.

RESULTS AND DISCUSSION

The InSe samples are mechanically exfoliated from InSe crystals onto a highly doped Si substrate with a 300 nm SiO_2 dielectric layer under ambient conditions. After exfoliation, we grow the surface OL on InSe flakes by employing UV-ozone treatment at 80 °C for 10 s. The atomic structure and chemical properties of the surface OL are examined by cross-sectional transmission electron microscopy (TEM) and energy-dispersive X-ray spectroscopy (EDX) mapping, as shown in Fig. 1a. Remarkably, the OL is uniformly grown, and the underlying InSe layers remain of a high-quality crystallinity, highlighting an atomically sharp and clean interface. The surface OL is amorphous with a thickness of 1 nm, ~1.3 times that of the single-layer InSe, implying that only the topmost monolayer is oxidized. The EDX mapping, which has been used to estimate the relative abundance of elements in the heterostructures, reveals that a substantial amount of Se atoms are substituted by O atoms within the OL regime, which is further

supported by X-ray photoelectron spectroscopy data (Supplementary Fig. S1). The In concentration remains constant up to the surface, suggesting the formation of substoichiometric InO_x . The TEM and EDX mapping clearly indicate the formation of a uniform OL generated from the topmost InSe monolayer, which we denote as an oxidized-monolayer (OML) from here forward. We note that in contrast to natively grown oxide (Supplementary Fig. S3) and oxygen plasma,²⁷ UV-ozone facilitates the strong oxidation of the InSe surface due to the presence of singlet oxygen atoms, which are chemically active.²⁸ The strong oxidizability could in principle lead to the domination of the vertical oxidation reaction over the lateral reaction triggered by the defects,²⁹ resulting in a uniform OML observed in our InSe samples.

The surface topography of the OML of InSe samples is characterized by using atomic force microscopy (AFM). The AFM images were acquired by the Peak-Force tapping mode using a sharp probe with a tip radius of 2 nm. (See Supplementary Information S2 for detail information.) The inset of Fig. 1b shows the AFM image of the OML that manifests a very uniform surface, signifying that even with a thickness of 1 nm, the surface OL is highly compatible with the underlying InSe. Figure 1b compares the histogram of the OML surface with that of a bulk hexagonal boron nitride (h-BN) flake and a SiO_2/Si substrate. Notably, the OML surface exhibits a very small roughness of 80 pm, confirming the high compatibility of the OML with the underlying InSe. It is noteworthy that the roughness of the oxidized InSe surface is comparable to that of h-BN (i.e., 90 pm), which exhibits an atomically smooth surface³⁰ and can be used in tunneling contacts for 2D-semiconductor-based devices.^{31,32} This ultra-

uniform surface thus suggests the viability of employing the OML as a tunneling barrier. As a comparison, nucleation sites are observable in the InSe samples not subjected to the UV-ozone treatment, which may be attributed to the native oxide that arises during exposure to the ambient atmosphere (Supplementary Figs. S3 and S4). Therefore, the uniform surface of the OML indicates a passivation and a stabilization effect resulting from the chemically stable surface oxide.³³

We further perform Raman spectroscopy to understand the crystal quality of the InSe sample before and after the UV-ozone treatment. As shown in Fig. 1c, we observe four characteristic Raman peaks in the pristine InSe sample at 117, 179, 200, and 228 cm^{-1} , corresponding to the out-of-plane (A_1) and in-plane (E) vibration modes.³⁴ After the UV-ozone treatment, these four characteristic Raman peaks show insignificant changes to their peak intensity and energy. The full width at half maxima before (after) the UV-ozone treatment are 2.9 (3.1), 5.7 (5.1), 2.3 (2.7), and 4.7 (4.8) for Raman modes at 117, 179, 200, and 228 cm^{-1} , respectively. The invariance of these Raman modes before and after the oxidation process clearly confirms that the crystal quality of the underlying InSe is negligibly affected by the UV-ozone treatment. No additional peaks corresponding to the oxide are observed, suggesting that the oxide is amorphous. To summarize, the comprehensive characterizations of TEM, AFM, and Raman spectroscopy show strong evidence of the ultra-uniform OML interfaced with the high-quality layered InSe underneath.

To understand the effects of introducing the ultrasmooth and uniform OML on the electrical properties of the InSe transistors, we fabricate back-gated devices with the contact structure illustrated in Fig. 2a. The thickness of the InSe flakes used for the devices ranges from 10 to 20 nm, as confirmed by AFM. The InSe samples are then transferred onto h-BN flakes by a dry transfer technique. We employ the h-BN flakes as the substrate for the InSe channel to reduce the extrinsic carrier scattering sources at the bottom interface (Supplementary Fig. S5).³⁵ The InSe/h-BN stacking structures are annealed in a furnace at $300\text{ }^\circ\text{C}$ with mixed gas (95% Ar and 5% H_2) to improve the quality of the InSe/h-BN interface and to remove the residual polymer at the surfaces. These InSe/h-BN samples are then oxidized by the UV-ozone process at a temperature ranging from 80 to $100\text{ }^\circ\text{C}$ for 10 s, followed by depositing electrical contacts (contact metal/Au of 15 nm/40 nm) with e-beam evaporation at a base pressure of 1×10^{-7} Torr. To attain high uniformity of the tunneling barrier, we employ a resist-free method to define the source and drain contacts³⁶ to avoid the potential resist residue in conventional lithography techniques, allowing us to study the FL-depinning effect accurately. For the resist-free fabrication method, we use the commercially available TEM grids to define the device channel by the shadow effect with the width ranging from 5 to 12 μm . The TEM grids are attached to a premade holder, which are then mounted on a home-made aligner. We then align the InSe flakes to the bar of the TEM grid under an optical microscope, subsequently followed by the metal deposition. We note that the TEM grid is not in contact with the InSe flake during the whole process, leading to the pristine condition of the InSe surface. The inset of Fig. 2b shows an optical microscopy (OM) image of a typical InSe device. All the electrical characterization are performed in a helium environment at a pressure of 20 Torr.

We first present the tunneling transport behavior of the OML-embedded InSe devices. As shown in Fig. 2b, the InSe devices constructed with UV-ozone processing temperatures of 80, 90, and $100\text{ }^\circ\text{C}$ exhibit nonlinear output curves (I_{ds} – V_{ds} curves). These nonlinear output curves can be well described by Simmons' model that manifests a cubic term in the V_{ds} dependence (inset in Fig. 2b and Supplementary Fig. S6), suggesting that the tunneling effect governs the charge transport as a result of introducing the OML. For higher processing temperatures, the I_{ds} decreases because of a larger contact resistance corresponding to a thicker OL, which is

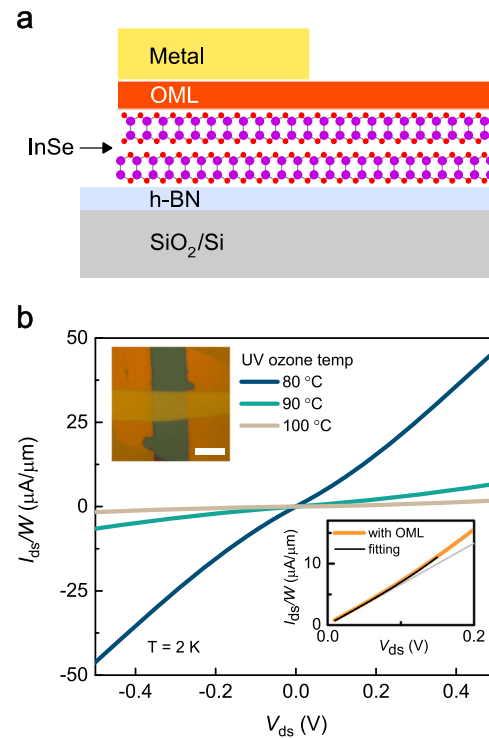


Fig. 2 Electrical properties of the InSe transistors embedded with oxidized-monolayer. **a** A schematic of the InSe device structure at the contact regime shows a surface oxidation layer embedded in between the contact metal and InSe. **b** The output curves of InSe devices utilizing UV-ozone processing temperatures of 80, 90, and $100\text{ }^\circ\text{C}$ for a duration of 10 s. The $V_{gs} = 80\text{ V}$, and the measured $T = 2\text{ K}$. Inset: (upper left) An OM image of a typical InSe device. The scale bar is 10 μm . (Lower right) The output curve for the InSe device utilizing a UV-ozone temperature of $80\text{ }^\circ\text{C}$ for 10 s, and the fitting curve calculated by Simmons' model. The gray line is a linear extrapolation of the output curve from the low-voltage regime.

consistent with the tunneling transport behavior in the OML-embedded InSe devices. The large I_{ds} of the InSe device with an OML grown at $80\text{ }^\circ\text{C}$ indicates the optimal tunneling efficiency with a low-contact barrier, therefore, this condition is employed to fabricate the OML for subsequent studies. Moreover, compared with the InSe sample without the OML, the InSe devices embedded with the OML exhibit a higher I_{ds} and lower barrier height (Supplementary Fig. S7), which is consistent with the tunneling contact behavior.²⁰

To evaluate the SBH of the MIS contact of the InSe devices, we conduct temperature (T)-dependent transport measurements and extract the SBH under flat-band gate bias conditions. Based on the thermionic emission model,⁹ the drain current injected through a reverse-biased Schottky barrier can be written as:

$$I_d = A^* T^{3/2} \exp\left(-\frac{E_A}{k_B T}\right) \left[1 - \exp\left(-\frac{qV_{ds}}{k_B T}\right)\right] \quad (1)$$

where A^* is Richardson's constant, k_B is the Boltzmann constant, T is the temperature, q is the elementary charge, E_A is the activation energy, and V_{ds} is the source-drain voltage. By fitting the Arrhenius plot of $I_d/T^{3/2}$, we can extract E_A , which represents the barrier height that the carriers have to overcome. The V_{ds} dependence of E_A is plotted to determine the SBH of the devices under the flat-band condition (Supplementary Fig. S8). The SBH extraction is found to only be applicable in the temperature range from 300 to 400 K, where the thermionic emission current dominates the carrier transport.¹⁵ Moreover, we note that the extracted SBH corresponds to an effective SBH that represents the

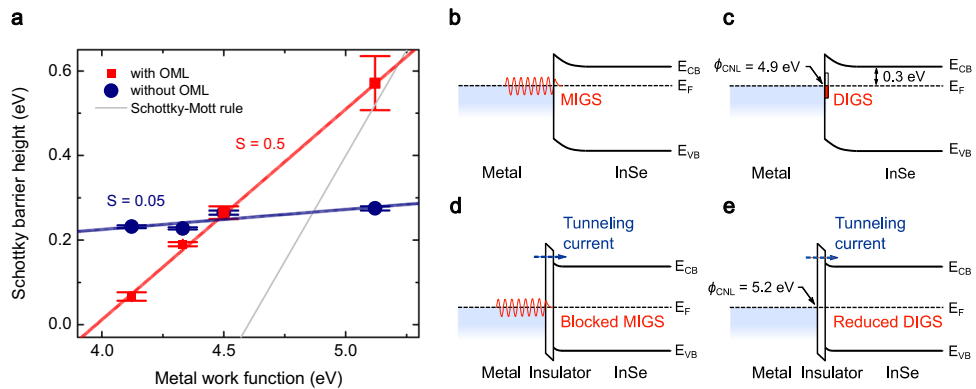


Fig. 3 Fermi-level depinning in the InSe transistors with the OML-embedded tunneling contact. **a** The SBH as a function of metal WF for the OML-embedded InSe devices and the control samples. The InSe devices with the OML-embedded tunneling contact manifest a large pinning factor of $S = 0.5$, indicating a pronounced FL depinning. The gray line shows the Schottky-Mott rule in the case of no FL pinning effect. Schematics of energy band diagrams at the metal/InSe interfaces show **b** the MIGS resulting from the decaying metal wave function tailing into InSe, and **c** the DIGS resulting from defect states. With the insertion the OML, the tunneling barrier can facilitate **d** attenuation of the gap states resulting from the penetrated metal wave functions, and **e** mitigation of the DIGS in metal/InSe interfaces. The ϕ_{CNL} is estimated to be 5.2 eV and 4.9 eV with and without the OML, respectively.

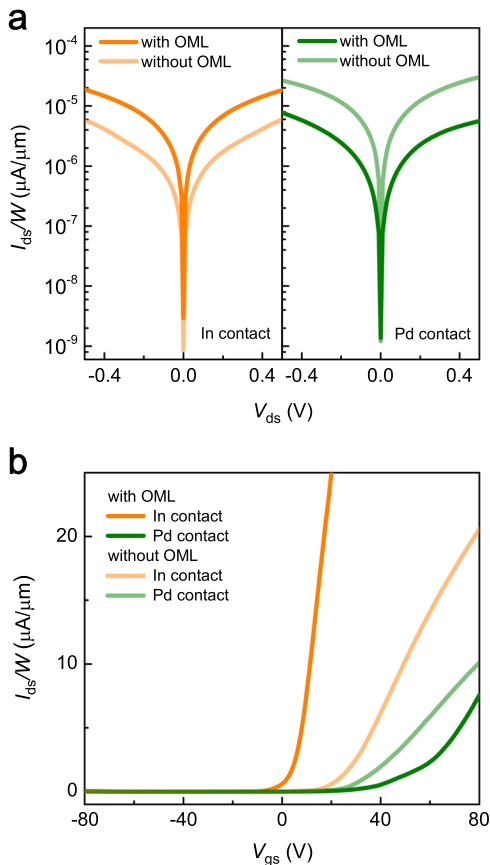


Fig. 4 Tunable transport characteristics controlled by the work function of the contact metal. **a** Semilogarithmic output curves for the InSe devices with In metal contacts at $T = 2$ K and $V_{\text{gs}} = 80$ V. The I_{ds} of InSe devices with the OML (orange line) is threefold larger than that of InSe devices without the OML (light orange line), indicating a reduced SBH. Semilogarithmic output curves for the InSe devices with Pd metal contacts at $T = 2$ K and $V_{\text{gs}} = 80$ V. The InSe device with the OML (green line) exhibits a decreased I_{ds} compared to that of the control sample (light green line). **b** The transfer curves of the InSe devices at $T = 2$ K with the OML (In contact: orange line; Pd contact: green line) and without the OML (In contact: light orange line; Pd contact: light green line). The applied source-drain voltage is 1 V. The changes in V_{th} and I_{ds} can be explained by the integration of the OML, further supporting the FL depinning in the InSe devices with the tunneling contact.

overall contact behavior because the insulating layer is not considered in the current–voltage characteristics described in Eq. (1).

We now discuss how the OML-embedded MIS contact affects the FL pinning effect in the InSe devices by examining the pinning factor and charge neutrality level.³⁷ The relation between the SBH and the metal WF can be depicted by the following equation:

$$\phi_{\text{Bn}} = S(\phi_m - \phi_{\text{CNL}}) + (\phi_{\text{CNL}} - \chi) = S\phi_m + b \quad (2)$$

where ϕ_{Bn} is the SBH for electrons, ϕ_m is the WF of the contact metal, χ is the electron affinity, and b is the y-intercept. S is the pinning factor and can be calculated by $S = d\phi_{\text{Bn}}/d\phi_m$, where $S = 1$ corresponds to the Schottky-Mott rule in which the SBH is simply determined by the difference between ϕ_m and χ , and $S = 0$ corresponds to absolute FL pinning, where the SBH is independent of the metal WF. The charge neutrality level, ϕ_{CNL} , denotes the energy of the surface states at which the FL of the metal electrodes is pinned. The ϕ_{CNL} can be estimated by the following expression, which is derived from Eq. (2):

$$\phi_{\text{CNL}} = \frac{\chi + b}{1 - S} \quad (3)$$

Figure 3a compares the SBH as a function of the metal WF for the OML-embedded InSe devices with that of the control samples. The S and ϕ_{CNL} are calculated using the following parameters: $\chi_{\text{InSe}} = 4.6$ eV,³⁸ $\phi_{m,\text{In}} = 4.12$ eV, $\phi_{m,\text{Ti}} = 4.33$ eV, $\phi_{m,\text{Cr}} = 4.5$ eV, and $\phi_{m,\text{Pd}} = 5.12$ eV.³⁹ Remarkably, the InSe transistors with the OML-embedded tunneling contact manifest a large pinning factor of $S = 0.5 \pm 0.01$, indicating a pronounced FL depinning. This result is in contrast to that of the control samples, revealing a strong FL pinning with $S = 0.05 \pm 0.02$. Moreover, due to the FL depinning, the modulation of the SBH by varying the WF of the contact metals (0.5 eV) is more substantial than that of the control samples (0.05 eV). We note that the FL depinning in layered semiconductors with a tunneling contact has not been realized before, highlighting the unique contact properties of the metal/insulator/layered-semiconductor interface.

The mechanism of the FL depinning in OML-embedded InSe transistors can be elucidated by examining the value of S and ϕ_{CNL} . First, a theoretical model considering the MIGS model predicts a pinning factor of $S = 0.2$ in an ideal metal/InSe interface.^{40,41} The OML-embedded InSe devices show a greater $S = 0.5$, indicating that the presence of the OML can suppress MIGS, as illustrated in Fig. 3b, d. Next, the ϕ_{CNL} is estimated by Eq. (3) to be 4.9 eV for the control samples. This ϕ_{CNL} is ~ 0.3 eV below the conduction band-edge (CBE) ($\chi_{\text{InSe}} = 4.6$ eV),³⁸ suggesting that

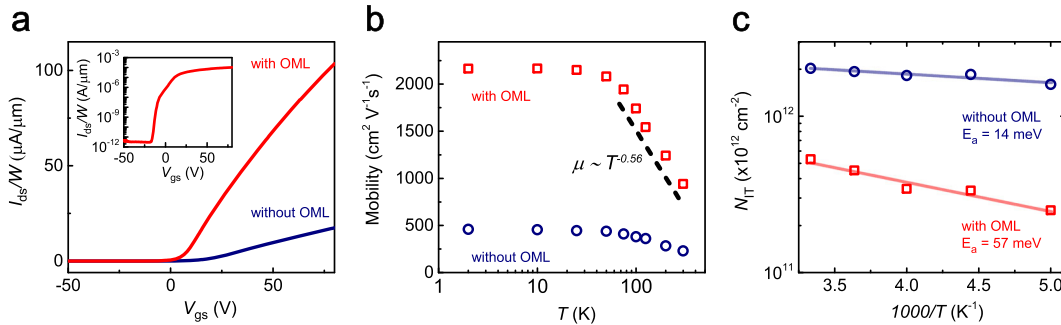


Fig. 5 Transport properties of the InSe transistors with the OML-embedded tunneling contact. Comparisons of the **a** transfer characteristics and **b** two-terminal field-effect mobilities (μ_{FE}) of the InSe devices with and without the OML-embedded tunneling contact. Inset: Semilogarithmic transfer characteristics of an InSe device with the OML, showing an ideal transistor behavior. The InSe transistor with the OML-embedded tunneling contact exhibits a high two-terminal μ_{FE} of $2160 \text{ cm}^2/\text{Vs}$ and a large on/off ratio of 10^8 at $T = 2 \text{ K}$. The source-drain voltage is 1 V . **c** A comparison of the surface trap densities of the InSe devices with and without the OML. The activation energies, E_a , of the InSe devices with and without the OML are extracted to be 57 and 14 meV, respectively.

the FL pinning in the control samples may be associated with defect states such as Se vacancies.⁴² With the OML, the ϕ_{CNL} increases to 5.2 eV, signifying that the DIGS corresponding to $\phi_{CNL} = 4.9 \text{ eV}$ are greatly suppressed, as depicted in Fig. 3c, e. It is noteworthy that the FL depinning resulting from the tunneling contact can be mainly attributed to the inherently dangling-bond-free nature of the layered materials, as well as the resist-free fabrication method of the metal contact. This clean interface and the high-quality InSe crystalline structure, as evidenced by the TEM characterizations, can mitigate the DIGS originating from the interfacial disorder. On the other hand, it has been reported that a tunneling barrier with a large band gap and small dielectric constant is beneficial to suppress FL pinning.¹⁸ Whether using an alternative ultrathin oxide within the MIS contact of the layered semiconductor can lead to even more complete FL depinning is worth further investigation.

Enabled by the FL depinning, we now show that the InSe devices with the tunneling contact manifest highly tunable transport characteristics controlled by the WF of the contact metal. Figure 4a compares the semilogarithmic output curves for InSe devices with In ($\phi_{m,In} = 4.12 \text{ eV}$) and Pd ($\phi_{m,Pd} = 5.12 \text{ eV}$) contact metals. In the case of the In contact, the I_{ds} of the OML-embedded InSe devices is increased by threefold, indicating a reduced SBH. In contrast, the InSe devices with the Pd contact exhibit a decreased I_{ds} and an increased contact barrier with the addition of the OML. This result is reasonable because for the Pd contact, we observe a larger SBH ($\phi_{Bn,Pd} \sim 0.57 \text{ eV}$) when the FL is not pinned compared with that of the pinning scenario ($\phi_{Bn,Pd} \sim 0.28 \text{ eV}$). On the other hand, the integration of the OML with the In contact leads to a small-energy difference between the In WF and the CBE when the FL depinning occurs.⁴³

Figure 4b compares the transfer curves ($I_{ds} - V_{gs}$ curves) of the OML-embedded InSe devices and the control samples at $T = 2 \text{ K}$. The control samples with In and Pd contact metals exhibit a comparable threshold voltage of $V_{th} = 30 \text{ V}$, suggesting the presence of the FL pinning effect. Interestingly, V_{th} shifts positively by 20 V and negatively by 25 V for larger (Pd) and smaller (In) WF metals, respectively. At low T , in the absence of the thermionic emission, V_{th} is associated with the difference between the metal WF and the CBE of InSe. The effective modulation of V_{th} by varying the WF of the contact metal thus confirms the occurrence of FL depinning in the InSe devices embedded with the OML. It is noted that the V_{th} for the OML-embedded InSe samples with the In contact is $\sim 0 \text{ V}$, which is reasonable because the energy difference between the In WF and the CBE is small.³⁵ On the other hand, owing to the high WF of Pd ($\phi_{m,Pd} = 5.12 \text{ eV}$) relative to that of InSe ($\phi_{m,InSe} = 4.7 \text{ eV}$), a large and positive V_{gs} is needed to electrostatically gate the InSe channel to attain the turn-on state.

The observed shifting in V_{th} is not caused by the doping effect of the surface oxide,⁴⁴ as verified by OML-embedded InSe devices with an additional ozone treatment that causes further oxidation layer (Supplementary Figs. S9 and S10). Therefore, the observed changes in V_{th} and I_{ds} due to the integration of the OML further substantiate the FL depinning in the InSe devices with the tunneling contact.

We have presented that the InSe devices with the tunneling contact enable the effective modulation of the SBH by alleviating FL pinning. This tunneling contact scheme can thus be utilized to improve the device performance by lowering the contact resistance. Accordingly, we demonstrate high-quality InSe devices with the OML-embedded tunneling contact by employing the In contact, which exhibits a small SBH of 65 meV (Fig. 3a). Figure 5a compares the transfer curves of an OML-embedded InSe device (sample A) and a control sample (sample B) at $T = 2 \text{ K}$ for $V_{ds} = 1 \text{ V}$. Both samples exhibit an n-type conduction behavior; however, sample A shows a high turn-on current of $103 \mu\text{A}/\mu\text{m}$ at $V_{gs} = 80 \text{ V}$, which is ~ 6 -times that of sample B. This enhanced I_{ds} can be attributed to a large tunneling contact area as a result of the uniform oxide layer⁴⁵ and a low energy barrier corresponding to the tunneling contact. The inset of Fig. 5a presents the logarithmic transfer curve of sample A, which exhibits a pronounced turn-on behavior. A large on/off ratio of 10^8 at $T = 2 \text{ K}$ (and 10^7 at $T = 300 \text{ K}$) is observed, indicating an ideal transistor behavior.

Figure 5b compares the two-terminal field-effect mobility (μ_{FE}) as a function of T for samples A and B in which the μ_{FE} is calculated by $\mu_{FE} = (1/V_{ds}C_{SiO_2})(L/W)(dI_{ds}/dV_{gs})$. Remarkably, sample A manifests a high two-terminal μ_{FE} of $2160 \text{ cm}^2/\text{Vs}$ at $T = 2 \text{ K}$ and $940 \text{ cm}^2/\text{Vs}$ at $T = 300 \text{ K}$. This μ_{FE} compares favorably with other layered-semiconductor-based transistors with the tunneling contact.^{31,32,46} The μ_{FE} of sample A is four-times that of the control sample, confirming the significance of introducing the OML into the metal/InSe interface. This enhancement in μ_{FE} can be attributed to the reduction in the contact barrier (Supplementary Fig. S7). At the high- T regime ($T = 200$ – 300 K), the T dependence of μ_{FE} can be described by $\mu_{ph} \propto T^{-\gamma}$ ($\gamma = 0.56$ and 0.52 for samples A and B, respectively), indicating a phonon-scattering-limited μ_{FE} .

We further examine the trap states in our InSe devices to understand the effect of the OML on the carrier transport properties. The trap density in a transistor can be estimated by $N_{tr} = C_{ox}\Delta V_{th}/q$, where C_{ox} is the gate capacitance of the h-BN/SiO₂ dielectric layer, ΔV_{th} is the shift in the V_{th} between the forward and backward sweeps of the transfer curves, and q is the elementary charge.⁴⁷ Figure 5c compares the trap density of the OML-embedded InSe devices with that of a control sample in an Arrhenius plot. We observe a larger trap density in the control

sample, which may be attributed to the formation of a native oxide or the adsorption of moisture.^{48,49} In contrast, the InSe device with the OML exhibits a very low trap density of $\sim 2 \times 10^{11} \text{ cm}^{-2}$, suggesting a higher interfacial quality. Moreover, the linear decrease in N_{IT} with lowering T in both devices is consistent with a thermally activated behavior.⁵⁰ The activation energy, E_{a} , of the InSe device with the OML is extracted to be 57 meV, suggesting that the trap states, albeit existing at a low density, negligibly affect the band-edge electrons due to the large energy difference between the trap states and the CBE. On the other hand, $E_{\text{a}} \sim 14 \text{ meV}$ is extracted for the control sample, indicating the presence of shallow traps. The small trap density and the large E_{a} of the OML-embedded InSe devices are both advantageous to the carrier transport in the channel, further validating the prominent transport characteristics (Supplementary Fig. S11).

In this work, we demonstrate a pronounced FL depinning in InSe transistors by employing a tunneling contact realized by a high-quality OML. Considering the great interest in layered-semiconductor-based devices, control of the contact properties is especially important for device applications. We show that the unique characteristics of layered semiconductors can be utilized to form an atomically thin, ultra-uniform OML. This OML is integrated into the tunneling contact of InSe transistors, leading to a strong FL depinning with $S = 0.5$ and an effective modulation of the SBH. Accordingly, the low-contact barrier is achieved with the tunneling contact and the In electrodes, enabling a high electron mobility of $2160 \text{ cm}^2/\text{Vs}$ in two-terminal InSe devices. The realization of FL depinning in high-mobility InSe transistors embedded with the OML inspires a feasible tunneling contact scheme for 2D-semiconductor-based electronic and optoelectronic applications.

METHODS

The InSe samples fabrication

For TEM, AFM, and Raman spectroscopy characterizations, the InSe samples are mechanically exfoliated from InSe crystals onto a highly doped Si substrate with a 300 nm SiO₂ dielectric layer under ambient conditions. After exfoliation, we grow the surface OL on InSe flakes by employing UV-ozone treatment at 80 °C for 10 s. For electrical characterization, we fabricate back-gated devices with the contact structure illustrated in Fig. 2a. The thickness of the InSe flakes used for the devices ranges from 10 to 20 nm, as confirmed by AFM. We exfoliate the InSe flakes onto polydimethylsiloxane (PDMS), which are then transferred onto pre-exfoliated h-BN flakes by a dry transfer technique. We employ the h-BN flakes as the substrate for the InSe channel to reduce the extrinsic carrier scattering sources at the bottom interface. The InSe/h-BN stacking structures are annealed in a furnace at 300 °C with mixed gas (95% Ar and 5% H₂) to improve the quality of the InSe/h-BN interface and to remove the residual polymer at the surfaces. These InSe/h-BN samples are then oxidized by the UV-ozone process at a temperature ranging from 80 to 100 °C for 10 s, followed by depositing electrical contacts (contact metal/Au of 15 nm/40 nm) with e-beam evaporation at a base pressure of $1 \times 10^{-7} \text{ Torr}$. To attain high uniformity of the tunneling barrier, we employ a resist-free method to define the source and drain contacts to avoid the potential resist residue in conventional lithography techniques, allowing us to study the FL-depinning effect accurately.

Measurement

All the electrical characterization are performed in a Physical Property Measurement System in a helium environment at a pressure of 20 Torr. The channel conductance was measured by using a Keithley 2636 and the gate voltage was applied by using a Keithley 2400.

DATA AVAILABILITY

Data presented in this work is available upon reasonable request from the corresponding author.

Received: 18 September 2019; Accepted: 25 November 2019;
Published online: 13 December 2019

REFERENCES

- Wang, Q. H., Kalantar-Zadeh, K., Kis, A., Coleman, J. N. & Strano, M. S. Electronics and optoelectronics of two-dimensional transition metal dichalcogenides. *Nat. Nanotechnol.* **7**, 699–712 (2012).
- Chhowalla, M., Jena, D. & Zhang, H. Two-dimensional semiconductors for transistors. *Nat. Rev. Mater.* **1**, 1–5 (2016).
- Jariwala, D., Sangwan, V. K., Lauhon, L. J., Marks, T. J. & Hersam, M. C. Emerging device applications for semiconducting two-dimensional transition metal dichalcogenides. *ACS Nano* **8**, 1102–1120 (2014).
- Sarkar, D. et al. A subthermionic tunnel field-effect transistor with an atomically thin channel. *Nature* **526**, 91–95 (2015).
- Liu, Y. Y., Stradins, P. & Wei, S. H. Van der Waals metal-semiconductor junction: weak Fermi level pinning enables effective tuning of Schottky barrier. *Sci. Adv.* **2**, 1–6 (2016).
- Liu, Y. et al. Approaching the Schottky-Mott limit in van der Waals metal-semiconductor junctions. *Nature* **557**, 696–700 (2018).
- Kang, J. H., Liu, W., Sarkar, D., Jena, D. & Banerjee, K. Computational study of metal contacts to monolayer transition-metal dichalcogenide semiconductors. *Phys. Rev. X* **4**, 1–4 (2014).
- Tung, R. T. The physics and chemistry of the Schottky barrier height. *Appl. Phys. Rev.* **1**, 1–54 (2014).
- Allain, A., Kang, J. H., Banerjee, K. & Kis, A. Electrical contacts to two-dimensional semiconductors. *Nat. Mater.* **14**, 1195–1205 (2015).
- Das, S., Chen, H. Y., Penumatcha, A. V. & Appenzeller, J. High performance multilayer MoS₂ transistors with scandium contacts. *Nano Lett.* **13**, 100–105 (2013).
- Schulman, D. S., Arnold, A. J. & Das, S. Contact engineering for 2D materials and devices. *Chem. Soc. Rev.* **47**, 3037–3058 (2018).
- Gerling, L. G. et al. Transition metal oxides as hole-selective contacts in silicon heterojunctions solar cells. *Sol. Energy Mater. Sol. Cells* **145**, 109–115 (2016).
- Tang, C. C. et al. Doped polymer semiconductors with ultrahigh and ultralow work functions for ohmic contacts. *Nature* **539**, 536–540 (2016).
- Brillson, L. J. & Lu, Y. C. ZnO Schottky barriers and Ohmic contacts. *J. Appl. Phys.* **109**, 1–3 (2011).
- Kim, C. et al. Fermi level pinning at electrical metal contacts of monolayer molybdenum dichalcogenides. *ACS Nano* **11**, 1588–1596 (2017).
- Bampoulis, P. et al. Defect dominated charge transport and fermi level pinning in MoS₂/metal contacts. *ACS Appl. Mater. Inter.* **9**, 19278–19286 (2017).
- Zhou, Y., Ogawa, M., Han, X. H. & Wang, K. L. Alleviation of Fermi-level pinning effect on metal/germanium interface by insertion of an ultrathin aluminum oxide. *Appl. Phys. Lett.* **93**, 1–3 (2008).
- Kobayashi, M., Kinoshita, A., Saraswat, K., Wong, H. S. P. & Nishi, Y. Fermi level depinning in metal/Ge Schottky junction for metal source/drain Ge metal-oxide-semiconductor field-effect-transistor application. *J. Appl. Phys.* **105**, 1–6 (2009).
- Nishimura, T., Kita, K. & Toriumi, A. A significant shift of Schottky barrier heights at strongly pinned metal/germanium interface by inserting an ultra-thin insulating film. *Appl. Phys. Express* **1**, 1–3 (2008).
- Lee, S., Tang, A., Aloni, S. & Wong, H. S. P. Statistical study on the Schottky barrier reduction of tunneling contacts to CVD synthesized MoS₂. *Nano Lett.* **16**, 276–281 (2016).
- Kim, G. S. et al. Schottky barrier height engineering for electrical contacts of multilayered MoS₂ transistors with reduction of metal-induced gap states. *ACS Nano* **12**, 6292–6300 (2018).
- Mleczko, M. J. et al. HfSe₂ and ZrSe₂: Two-dimensional semiconductors with native high-kappa oxides. *Sci. Adv.* **3**, 1–9 (2017).
- Yamamoto, M. et al. Self-limiting layer-by-layer oxidation of atomically thin WSe₂. *Nano Lett.* **15**, 2067–2073 (2015).
- Bandurin, D. A. et al. High electron mobility, quantum Hall effect and anomalous optical response in atomically thin InSe. *Nat. Nanotechnol.* **12**, 223–227 (2017).
- Feng, W., Zheng, W., Cao, W. & Hu, P. Back gated multilayer InSe transistors with enhanced carrier mobilities via the suppression of carrier scattering from a dielectric interface. *Adv. Mater.* **26**, 6587–6593 (2014).
- Mudd, G. W. et al. Tuning the bandgap of exfoliated InSe nanosheets by quantum confinement. *Adv. Mater.* **25**, 5714–5718 (2013).
- Chang, Y. R. et al. Surface oxidation doping to enhance photogenerated carrier separation efficiency for ultrahigh gain indium selenide photodetector. *ACS Photonics* **4**, 2930–2936 (2017).
- DeRosa, M. C. & Crutchley, R. J. Photosensitized singlet oxygen and its applications. *Coord. Chem. Rev.* **233**, 351–371 (2002).

29. Yamamoto, M., Einstein, T. L., Fuhrer, M. S. & Cullen, W. G. Anisotropic etching of atomically thin MoS₂. *J. Phys. Chem. C* **117**, 25643–25649 (2013).

30. Dean, C. R. et al. Boron nitride substrates for high-quality graphene electronics. *Nat. Nanotechnol.* **5**, 722–726 (2010).

31. Wang, J. L. et al. High mobility MoS₂ transistor with low schottky barrier contact by using atomic thick h-BN as a tunneling layer. *Adv. Mater.* **28**, 8302–8308 (2016).

32. Cui, X. et al. Low-temperature ohmic contact to monolayer MoS₂ by van der Waals bonded Co/h-BN electrodes. *Nano Lett.* **17**, 4781–4786 (2017).

33. Nan, H. Y. et al. Producing air-stable InSe nanosheet through mild oxygen plasma treatment. *Semicond. Sci. Technol.* **33**, 1–7 (2018).

34. Sanchez-Royo, J. F. et al. Electronic structure, optical properties, and lattice dynamics in atomically thin indium selenide flakes. *Nano Res.* **7**, 1556–1568 (2014).

35. Huang, Y. T. et al. High-performance InSe transistors with ohmic contact enabled by nonrectifying barrier-type indium electrodes. *ACS Appl. Mater. Inter.* **10**, 33450–33456 (2018).

36. Chen, S. Y., Ho, P. H., Shieh, R. J., Chen, C. W. & Wang, W. H. Transport/magnetotransport of high-performance graphene transistors on organic molecule-functionalized substrates. *Nano Lett.* **12**, 964–969 (2012).

37. Robertson, J. Band offsets, Schottky barrier heights, and their effects on electronic devices. *J. Vac. Sci. Technol. A* **31**, 1–18 (2013).

38. Kudrynskyi, Z. R. et al. Giant quantum hall plateau in graphene coupled to an InSe van der Waals crystal. *Phys. Rev. Lett.* **119**, 1–5 (2017).

39. Michaelson, H. B. The work function of the elements and its periodicity. *J. Appl. Phys.* **48**, 4729–4733 (1977).

40. Brudnyi, V. N., Sarkisov, S. Y. & Kosobutsky, A. V. Electronic properties of GaSe, InSe, GaS and GaTe layered semiconductors: charge neutrality level and interface barrier heights. *Semicond. Sci. Technol.* **30**, 1–19 (2015).

41. Guo, Y. Z. & Robertson, J. Band structure, band offsets, substitutional doping, and Schottky barriers of bulk and monolayer InSe. *Phys. Rev. Mater.* **1**, 1–9 (2017).

42. Kistanov, A. A., Cai, Y., Zhou, K., Dmitriev, S. V. & Zhang, Y. W. Atomic-scale mechanisms of defect- and light-induced oxidation and degradation of InSe. *J. Mater. Chem. C* **6**, 518–525 (2018).

43. Zheng, S., Lu, H. C., Liu, H., Liu, D. M. & Robertson, J. Insertion of an ultrathin Al₂O₃ interfacial layer for Schottky barrier height reduction in WS₂ field-effect transistors. *Nanoscale* **11**, 4811–4821 (2019).

44. Cai, L. L. et al. Rapid flame synthesis of atomically thin MoO₃ down to monolayer thickness for effective hole doping of WSe₂. *Nano Lett.* **17**, 3854–3861 (2017).

45. Giannazzo, F. et al. Ambipolar MoS₂ transistors by nanoscale tailoring of schottky barrier using oxygen plasma functionalization. *ACS Appl. Mater. Inter.* **9**, 23164–23174 (2017).

46. Avsar, A. et al. van der Waals bonded Co/h-BN contacts to ultrathin black phosphorus devices. *Nano Lett.* **17**, 5361–5367 (2017).

47. Yamamoto, M., Ueno, K. & Tsukagoshi, K. Pronounced photogating effect in atomically thin WSe₂ with a self-limiting surface oxide layer. *Appl. Phys. Lett.* **112**, 1–5 (2018).

48. Ho, P. H. et al. High-mobility InSe transistors: the role of surface oxides. *ACS Nano* **11**, 7362–7370 (2017).

49. Late, D. J., Liu, B., Matte, H. S. S. R., Dravid, V. P. & Rao, C. N. R. Hysteresis in single-layer MoS₂ field effect transistors. *ACS Nano* **6**, 5635–5641 (2012).

ACKNOWLEDGEMENTS

This work was supported by the Ministry of Science and Technology of Taiwan, R.O.C. under contract numbers MOST 103-2112-M-001-020-MY3.

AUTHOR CONTRIBUTIONS

Y.H.C., C.Y.C. and W.H.W. conceived the research and designed the experiment. Y.H.C. performed device fabrication, characterizations, and data analysis. S.Y.C. contributed to the Raman spectroscopy measurement and analysis. J.S.D.R. and H.S.C. performed the AFM measurement and analysis. H.T.L. contributed the Raman spectroscopy measurement. K.W. and T.T. contributed h-BN material. R.S. and F.C.C. contributed InSe material. All authors discussed the results and commented on the manuscript. Y. H.C., C.Y.C., S.Y.C. and W.H.W. wrote the manuscript.

COMPETING INTERESTS

The authors declare no competing interests.

ADDITIONAL INFORMATION

Supplementary information is available for this paper at <https://doi.org/10.1038/s41699-019-0133-3>.

Correspondence and requests for materials should be addressed to W.H.W.

Reprints and permission information is available at <http://www.nature.com/reprints>

Publisher's note Springer Nature remains neutral with regard to jurisdictional claims in published maps and institutional affiliations.



Open Access This article is licensed under a Creative Commons Attribution 4.0 International License, which permits use, sharing, adaptation, distribution and reproduction in any medium or format, as long as you give appropriate credit to the original author(s) and the source, provide a link to the Creative Commons license, and indicate if changes were made. The images or other third party material in this article are included in the article's Creative Commons license, unless indicated otherwise in a credit line to the material. If material is not included in the article's Creative Commons license and your intended use is not permitted by statutory regulation or exceeds the permitted use, you will need to obtain permission directly from the copyright holder. To view a copy of this license, visit <http://creativecommons.org/licenses/by/4.0/>.

© The Author(s) 2019